IEEE Access
Multidisciplinary | Rapid Review | Open Access Journal

Received January 22, 2022, accepted March 7, 2022, date of publication March 15, 2022, date of current version March 22, 2022.

Digital Object Identifier 10.1109/ACCESS.2022.3159231

A Machine Learning-Based Method for Wind Fields Forecasting Utilizing GNSS Radio Occultation Data

XUEZHAO CHU[1,2], WEIHUA BAI[3,4,5,6,7], YUEQIANG SUN[3,4,5,6,7], WEI LI[3,4,6,7], CONGLIANG LIU[3,4,6,7], AND HONGQING SONG[1,2]

[1]School of Civil and Resource Engineering, University of Science and Technology Beijing, Beijing 100083, China
[2]National and Local Joint Engineering Laboratory for Big Data Analysis and Computer Technology, Beijing 100190, China
[3]National Space Science Center, Chinese Academy of Sciences (NSSC/CAS), Beijing 100190, China
[4]Beijing Key Laboratory of Space Environment Exploration, Beijing 100190, China
[5]School of Astronomy and Space Science, University of Chinese Academy of Sciences, Beijing 100049, China
[6]Joint Laboratory on Occultations for Atmosphere and Climate (JLOAC), NSSC/CAS and University of Graz, Beijing 100190, China
[7]Key Laboratory of Science and Technology on Space Environment Situational Awareness, Chinese Academy of Sciences, Beijing 100190, China

Corresponding author: Hongqing Song (songhongqing@ustb.edu.cn)

This work was supported jointly by the Youth Cross Team Scientific Research Project of the Chinese Academy of Sciences (JCTD-2021-10), the National Natural Science Foundation of China under Grant no. 42074042, the Feng Yun 3 (FY-3) Global Navigation Satellite System Occultation Sounder (GNOS and GNOS II) Development and Manufacture Project led by the National Space Science Center, Chinese Academy of Sciences (NSSC/CAS).

ABSTRACT With the development of computer technology and expanding environmental issues, machine learning has received more and more attention in the field of weather forecasting. Global Navigation Satellite System-Radio Occultation(GNSS-RO) technology is a kind of remote sensing technology. This investigation proposes an alternative to numerical weather forecasting model. The new method is based on machine learning utilizing GNSS-RO data to forecast the wind field in the Beijing-Tianjin-Hebei region of China. The dataset including temperature, humidity, pressure, wind speed and direction was obtained by numerical calculation in terms of historical monitoring data in Beijing-Tianjin-Hebei region. Then the models of wind fields forecasting based on machine learning were established with different neural network including Long Short-Term Memory (LSTM), Convolutional Neural Network (CNN) and Deep Neural Networks (DNN). The prediction performance of different models was analyzed. The results demonstrate that LSTM and CNN have better performance on predicting the wind field than Deep Neural Networks. The wind speed error is about 1.4m/s, and the wind direction error is about 30°. Moreover, the time required for neural network to predict a new sample is about 1 second, which is only 0.2% of the prediction time compared with numerical model. Finally, the machine learning model can be used to predict the wind field effectively, with GNSS-RO data as the input in application. This paper pro-vides a new method in sight to use machine learning to forecast the regional wind field utilizing GNSS-RO data.

INDEX TERMS Wind fields forecasting, machine learning, GNSS-RO, long short-term memory (LSTM), convolutional neural networks (CNN).

I. INTRODUCTION

In recent years, with the development of the industrialization, the environmental problems caused by industrial production, especially the air pollution problems, have a serious threat to our lives [1]. The wind field has a direct impact on air pollution [2]. In order to predict and pre-warning air pollution, it is of great significance to propose an effective method to predict the regional wind field.

The associate editor coordinating the review of this manuscript and approving it for publication was Yongming Li.

With the development of the observation technology, the accuracy and resolution of meteorological data used for wind field prediction have been greatly improved [3]. Global Navigation Satellite System-Radio Occultation(GNSS-RO) is a remote sensing technology, which has the advantages of high precision, high vertical resolution, self-correction, global coverage, all-weather, real-time, long-term stability and low cost [4]. An occultation event is that one GNSS satellite receives the signal transmitted by an-other LEO satellite in a time period. Each occultation event corresponds to a profile. In the aspects of providing temperature, humidity,

pressure profile monitoring means, GNSS-RO technology plays an irreplaceable role due to the global uniform distribution and high vertical resolution [5]. It has great scientific significance for weather forecasting and provides an extensive application prospect. Mueller *et al.* [6] assessed the potential impact of GNSS-RO on forecasting tropical cyclone track, maximum 10-m wind speed and integrated kinetic energy. The track model prediction error was similar to those of the National Hurricane Center, and the maximum 10-m wind speed and integrated kinetic energy error showed similar results. Allabakash and Lim [7] used the planetary boundary layer height obtained from GNSS-RO dataset to examine its impact on the temperature, relative humidity, surface pressure and wind speed of the Korean peninsula and surrounding waters. Liou *et al.* [8] found the height dependence of GNSS-RO data and the gravity waves and estimated the horizontal wind speed perturbations. The results are in good agreement with radiosonde data. Based on the simulated observations, Ying and Zhang [9] explored the potentials in improving the prediction of weather systems and the accuracy of wind speed, temperature and humidity over 200km.

The observation data of temperature, humidity and pressure can be collected from GNSS-RO, so as to simulate and predict the wind field and reflect the distribution of the wind field [10]. These observation data can be used as boundary and initial conditions to forecast meteorological parameters with atmospheric physics model [11]. A widely used numerical weather prediction model is WRF (weather research and forecasting) model, which can reflect the real atmospheric data or ideal atmospheric environment by simulation [12]. It is widely used in the research of forecasting wind speed, temperature, humidity and pressure [13]. Pokhrel *et al.* [14] used WRF to simulate the changes of wind speed, rainfall and other meteorological data caused by Hurricane Maria. This study filled the gap of the hydrometeorological processes due to the limited observational data. Díaz Fernández *et al.* [15] used WRF model to simulate five atmospheric variables, including wind direction, wind speed, atmospheric stability, liquid water content and temperature, to forecast and warn mountain waves, wave clouds and icing events. Three prediction methods were validated against satellite images. Yang *et al.* [16] configured Microwave Radiation Imager (MWRI) radiance data in WRF model's data assimilation system to improve the analysis of typhoon central sea level pressure and wind speed and compared with European Centre for Medium-Range Weather Forecasts (ECMWF) analysis data.

Compared with the traditional methods, machine learning model does not need to build control equations to describe the atmospheric motion, which can greatly reduce the time required for prediction [17]–[19]. Machine learning model can analyze meteorological data to achieve the purpose of prediction and is more and more used in the of wind field prediction [20]–[23]. Wang *et al.* [24] proposed and compared 8 methods of wind speed prediction based on machine learning. They improved the comb-dirmo model to predict the wind field and achieved good results. Neshat *et al.* [25] adopted a new hybrid deep learning-based method to train and test the winds over the Baltic Sea and proved that the model is superior to other six machine learning models and seven hybrid models. The new model was combined with bi-directional long short-term memory neural network, effective hierarchical evolutionary decomposition technology and improved generalized normal distribution optimization algorithm. Dong *et al.* [26] proposed a new hybrid machine learning method. In the study, It solved the poor interpretability and robustness which were caused by the non-convexity of loss function. The local convolution neural network was adopted to keep the convexity of the loss function, effectively solved the convergence problem of non-convexity, and improved the accuracy and stability of wind speed prediction. Inspired by the residual U-net architecture of convolutional neural network, Shivam *et al.* [27] proposed a Res-DCCNN model for wind speed prediction and verified the robustness and accuracy of the model on real wind speed datasets with different probability distributions.

In this paper, a machine learning-based method for wind fields forecasting utilizing GNSS-RO data is proposed. The GNSS-RO technology and deep learning algorithm are combined to forecast the wind field in Beijing-Tianjin-Hebei region. The prediction of wind field in Beijing-Tianjin-Hebei region is divided into the following four steps: Firstly, WRF is used to predict the wind field in Beijing-Tianjin-Hebei region in previous years with the historical data from the European Centre for Medium-Range Weather Forecasts; Secondly, the datasets including temperature, humidity, pressure, wind speed and direction are obtained from the simulation results, which are treated as the characteristic data for the input of machine learning. The deep learning models are established, trained and tested with the dataset; Thirdly, the accuracy and calculation time are compared between different neural networks, such as Long Short-Term Memory (LSTM), Convolutional Neural Networks (CNN) and Deep Neural Networks (DNN); Finally, the wind field is predicted by the deep learning model with the dataset which includes temperature, humidity and pressure obtained from GNSS-RO data.

II. METHODOLOGY

A. GNSS RADIO OCCULTATION

Global Navigation Satellite System (GNSS)/Low Earth Orbit Satellite (LEO) Radio Occultation Technology has become a new method to detect the earth environment parameters [28]–[33]. The main navigation satellite systems in the world include the Global Positioning System (GPS), the Galileo system cooperated by the EU and China, the Global Navigation Satellite System of Russia, and China's BeiDou Navigation Satellite System. With the improvement of global navigation, the radio occultation technology has been further developed.

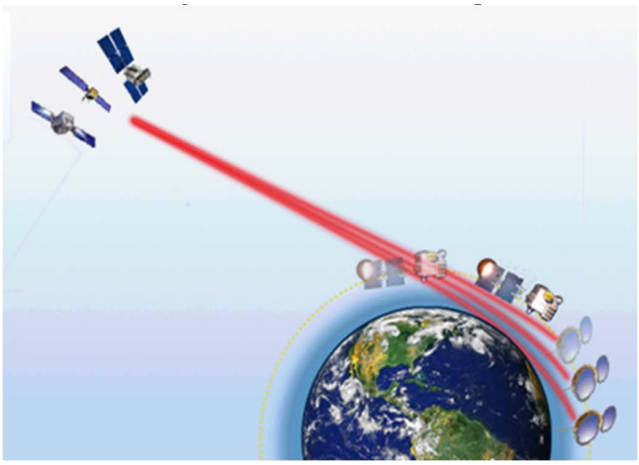

FIGURE 1. Diagram of radio occultation process. ©UCAR.

GNSS radio occultation technology began in the 1990s [5]. In 1995, the successful launch of American LEO satellite verified the feasibility of using navigation satellite and LEO satellite to detect the earth's atmosphere [5]. GNSS radio occultation can obtain the information of electron density of ionospheric and atmospheric refractive index, and then retrieve the atmospheric temperature, pressure and humidity from the refractive index [34]–[39]. The electromagnetic wave signal from GNSS satellite passes through the atmosphere and is received by GNSS receiver installed on LEO satellite. Due to the inhomogeneity of the atmosphere, the atmosphere will produce refraction effect on the electromagnetic wave emitted by GNSS, which makes the electromagnetic wave bend. The receiver on LEO satellite can get accurate phase delay and signal-to-noise ratio. By using Doppler observation equation and ephemeris of LEO satellite and navigation satellite, the additional phase delay and amplitude data of signal are de-rived, and the variation of bending angle with altitude is obtained; On this foundation, by using Abel transform, the atmospheric refractive index can be obtained by bending angle, and then the atmospheric parameters such as temperature, humidity and pressure can be deduced. Figure 1 is a schematic diagram of the radio occultation process.

GNSS-RO technology has the advantages of high precision, high vertical resolution, self calibration, global coverage, all-weather, real-time, long-term stability and low cost. It can provide temperature, humidity, pressure profile which have the characteristic of global uniform distribution and high vertical resolution [40]. The data of temperature, humidity and pressure is able to be used to calculate the atmospheric wind field and reflect the distribution of the atmospheric wind field [41]. These data can be processed from radio occultation to forecast meteorological parameters utilizing prediction model.

B. NEURAL NETWORK MODELS

This experiment is based on the server with the memory size of 64G and 128 CPU core numbers. The study used python to build neural networks in the PyCharm, an integrated development environment. Karas is one of the python deep learning application programming interfaces, the sequential model of which was used to set neural network parameters.

DNN uses back propagation algorithm, which is composed of multi-layer perceptron [42], [43]. The basic idea of DNN is the gradient descent method, which adjusts the parameters of neural network, gradually reduces the error mean square deviation of the actual output value and the expected value of neural network. Finally, it makes the error mean square deviation reach the minimum, so as to get the output value closest to the expected value [44]–[46]. DNN algorithm includes two stages: signal forward propagation and error back propagation. The training results are recorded in the form of weights and thresholds of each neuron. The neural network is continuously trained by repeating the two stages of forward propagation and back propagation, so that the predicted value of wind speed and direction is the closest to the true value. Keras was used in DNN. The input layer of the model is composed of Temperature, humidity and pressure data of 245 points distributed around the predicted location. The hidden layer is designed as three layers, with 64 neurons in each layer. Finally, the number of neurons in the out-put layer is 1. Different models output meridional wind, zonal wind and wind direction respectively. We have carried relevant experiments and proved that the prediction effect of DNN in this study is similar to that of random forest. Therefore, we no longer take random forest as the research method alone in this paper.

Convolution neural network (CNN) is a kind of feed-forward neural network, which is one of the most widely used deep learning algorithms [47]. But different from DNN, convolution neural network consists of the following five parts: input layers, convolution layers, pooling layers, fully connected layers and output layers. The advantage with respect to the prediction performance of convolution neural network is that it can extract features of input by convolution and pooling compared with other neural networks. Features refer to the wind speed and direction obtained from temperature, humidity and pressure. The convolution layer extracts feature by dot product of the convolution kernel and the data of the training set. The pooling layer processes the data from the convolution layer to reduce the feature dimension. Due to the convolution layer and pooling layer, convolutional neural network has good performance in extracting input data features.

The input layer of convolutional neural network can process multi-dimensional data and contain multiple channels. The hidden layer of convolutional neural network includes convolution layer and pooling layer, which is a unique structural feature of convolutional neural network [48], [49]. The output of the convolution layer is represented as follows:

$$Z_{i,j}^{l+1} = F_1\left(\sum_{q=1}^{k^l} w_{i,q}^l Z_{i,r}^l + b_{i,j}^l\right), \tag{1}$$

$$r = (j-1) * s^l, \tag{2}$$

where $Z_{i,j}^{l}$ signifies jth input of ith period in lth layer, $w_{i,q}^{l}$ signifies qth weight of ith period in lth layer, $b_{i,j}^{l}$ signifies jth bias of ith period in lth layer, F_1 signifies the activation function, k^l and s^l signify the kernel size and the stride in lth layer. The output of the pooling layer is represented as follows:

$$Z_{i,j}^{l+1} = F_2\left(Z_{i,r+1}^{l}, Z_{i,r+2}^{l}, Z_{i,r+3}^{l}, \ldots, Z_{i,r+k^l}^{l}\right), \quad (3)$$

$$r = (j-1) * s^l, \quad (4)$$

where $Z_{i,j}^{l}$ signifies jth input of $i$thn period in lth layer, $w_{i,q}^{l}$ signifies qth weight of ith period in lth layer, $b_{i,j}^{l}$ signifies jth bias of ith period in lth layer, F_2 signifies the function that find the maximum or minimum value in these variables, k^l and s^l signify the kernel size and the stride in lth layer.

The temperature (data format: 5 × 7 × 7), humidity (data format: 5 × 7 × 7), and pressure data (data format: 5 × 7 × 7) were integrated and reshaped to a dataset (data format: 3 × 5 × 49). Two convolutional layers were used to extract data features, with a number of 128 convolution kernels respectively. The size of the convolution kernel is 3 × 5 and 2 × 3 respectively. And the max pooling function and a kernel size of 2 × 2 were used in the two pooling layers. At last, the fully connected layer is designed as three hidden layers, with 64 neurons in each layer.

Long Short-Term Memory (LSTM) neural network [50]–[53] is a kind of Recurrent Neural Network (RNN). When dealing with some events related to the occurrence time, the traditional CNN cannot solve the problems caused by the correlation be-tween different time series data. Therefore, LSTM has become a better choice when dealing with time series problems. LSTM is a kind of particular structure to selectively let information pass through. LSTM stores the information of the past event with cells. It protects and controls the information by three gate structures: input gate, forgetting gate and output gate. The function of the forgetting gate is to select the discarded in-formation from the cells. The forgetting gate will read the output data and input data of the previous step and output a number from 0 to 1. The number indicates the degree of information retention, and 1 means complete retention. The output of the forgetting gate can be represented as follows:

$$f_t = \sigma\left(w_f \cdot [h_{t-1}, x_t] + b_f\right), \quad (5)$$

where σ is the sigmoid function, h_{t-1} is the output data of $(t-1)$th period, x_t is the input data of tth period, w_f is the weight and b_f is bias.

The function of the input gate is to select new data to store in the cell. The sigmoid layer is used to select what information needs to be updated, and the activation layer is used to generate the content of the updated information $\tilde{C}_t$. With the output of forgetting gate, the old cell state C_{t-1} is updated to C_t. The equation of $\tilde{C}_t$, and C_t are represented as follows:

$$\tilde{C}_t = F\left(w_C \cdot [h_{t-1}, x_t] + b_C\right), \quad (6)$$

$$C_t = f_t \cdot C_{t-1} + i_t \cdot \tilde{C}_t, \quad (7)$$

$$i_t = \sigma\left(w_i \cdot [h_{t-1}, x_t] + b_i\right), \quad (8)$$

where σ is the sigmoid function, h_{t-1} is the output data of $(t-1)$th period, x_t is the input data of tth period, w_C is the weight and b_C is bias, F is the activation function.

The function of the output gate is to determine the output value. The sigmoid layer is used to select the cell state to output, and the activation layer is used to process the cell state C_t. The multiplication of the two parts is the output value of the cell state after screening. The output of the cell is represented as follows:

$$o_t = \sigma\left(w_o \cdot [h_{t-1}, x_t] + b_o\right), \quad (9)$$

$$h_t = o_t \cdot F(C_t), \quad (10)$$

where h_t is the output, h_t is the output data of tth period, x_t is the input data of tth period, w_o is the weight and b_o is bias, F is the activation function.

Two LSTM layers and one fully connected layer were used in LSTM model. One LSTM layer had 64 neurons and the other had 128 neurons. And the fully connected layer had 64 neurons.

The error gradient is used to obtain the direction and amplitude of network parameter update in network training. Due to the error gradient is repeatedly multiplied by the gradient value greater than 1.0 in the update, the gradient value increases exponentially, and a very large gradient is accumulated over time. It is called gradient explosion. However, due to the forgetting gate, the LSTM model will change the weight of the historical signal independently, so that the long-distance gradient will not disappear completely, which solves the problem of gradient disappearance in RNN.

The hyperparameters used in the study are manually turned to achieve better training performance.

C. MODEL EVALUATION

According to the verification method for wind forecast issued by China Meteorological Administration, in order to evaluate the prediction performance of different forecasting models, root mean square error is used as the standard to test the prediction error of wind speed, and the average absolute error is used as the standard to test the prediction error of wind direction.

The average absolute value of the error between the predicted wind direction angle and the actual wind direction angle is used to evaluate the performance of wind direction forecast. The equation of MAE is represented as follows:

$$MAE_d = \frac{1}{NF_d}\sum_{i=1}^{NF_d} \min\left(\left|F_{d,i} - O_{d,i}\right|, 360 - \left|F_{d,i} - O_{d,i}\right|\right), \quad (11)$$

where MAE_d signifies the mean absolute error of wind direction forecast, NF_d signifies the total number of times of wind direction forecast, i signifies the number of times of wind direction forecast, $F_{d,i}$ signifies the predicted value of

the ith wind direction, $O_{d,i}$ signifies the actual value of the ith wind direction.

The standard deviation of the prediction error is used to evaluate the performance of wind speed forecast. The equation of $RMSE$ is represented as follows:

$$RMSE_s = \sqrt{\frac{1}{NF_s}\sum_{j=1}^{NF_s}\left(F_{s,j} - O_{s,j}\right)^2}, \tag{12}$$

where $RMSE_s$ signifies the root mean square error of wind speed forecast, NF_s is the total number of times of wind speed forecast, j signifies the number of times of wind speed forecast, $F_{s,j}$ signifies the predicted value of the jth wind speed. $O_{s,j}$ signifies the actual value of the jth wind speed.

III. PROCEDURE

A. DATA COLLECTION

The Beijing-Tianjin-Hebei region is located in the center of the Bohai Rim of Northeast China. It is the largest and most dynamic region in northern China. The Beijing-Tianjin-Hebei region bears a great mission in promoting China's economic rise. But the weather and pollution in the Beijing-Tianjin-Hebei region have affected its development and the quality of life of local residents. Therefore, it is very necessary to forecast the wind field in the Beijing-Tianjin-Hebei region, which has an important impact on weather and air pollution. In this paper, ECMWF Re-Analysis(ERA)-interim historical data was used to predict the wind field in Beijing-Tianjin-Hebei region from June 2018 to July 2019 by numerical model. The initial data came from the European Centre for Medium-Range Weather Forecasts. And then, the machine learning models were established based on the dataset, which was collected from the numerical model. In application, the temperature, humidity and pressure data are extracted from cosmic occultation data as the inputs of neural network, and the wind field in Beijing-Tianjin-Hebei region is predicted by the machine learning model which has the best performance among the different models.

1) GNSS-RO DATA

GNSS radio occultation was developed in the 1990s and has been used to study the earth's atmosphere in recent years. The data product we used is wetPrf. In this paper, cosmic occultation data from June 2018 to July 2019 are selected. The data is di-vided according to different time period.

The data are interpolated to a grid with a step of 100 meters. In each time period, the temperature, humidity and pressure of each profile in the vertical direction are interpolated according to the ETA layer. In the horizontal direction, the temperature, humidity and pressure of each isobaric surface are interpolated according to the grid division of the output file of numerical model. If there are not enough occultation events in the period of time, the accuracy of meteorological parameters obtained by interpolation is not great enough. Therefore, the wind field is predicted in a period when more than 5 occultation events occur. The meteorological parameters (temperature, humidity and pressure) at each grid point are extracted, output and saved, so that they can be used as the input of neural network for wind field prediction. That is to say, GNSS-RO data can be processed into a format that can be input into neural network and trained. GNSS-RO data in a certain time period can be arranged and the neural network model which has been trained and tested is used to predict the wind field in Beijing Tianjin Hebei region in the next few hours.

2) WIND FIELD DATA

GNSS-RO data can provide global uniform distribution and high vertical resolution data of temperature, humidity and pressure; therefore, GNSS-RO data is used as the input of the model in the wind field prediction in application. However, different from in the prediction process in application, GNSS-RO data cannot provide enough datasets due to the limitation of its own technical means in the training process of ma-chine learning. Therefore, ERA-interim data with rich data is more suitable for the training process of machine learning.

The ERA-interim dataset from ECMWF is a reanalysis of the abundant global atmospheric data since 1979. However, the shortest time interval of ERA-interim reanalysis is 6 hours and the highest spatial resolution of ERA-interim data is 0.125 ° × 0.125°. It cannot meet the requirements of specific prediction time and spatial resolution in some practical applications; But the numerical model can set the corresponding time and space resolution to simulate and predict the wind field according to the specific requirements. Therefore, this paper needs to take ERA-interim data as the initial field and use the numerical model to simulate and predict the wind field with a certain spatial and temporal resolution. The meteorological data can be got from the prediction results of the numerical model. All of these provide datasets for machine learning training.

ERA-interim is divided into different types according to the classification standard of initial field data. The classification standard includes model level, potential temperature, potential vorticity, pressure level and surface dataset. In this paper, pressure level data and surface data are selected as the initial field for numerical simulation. The horizontal coverage is from 50°N to 30°N and from 100°E to 130°E。 The real-time data is on 00:00, 06:00, 12:00 and 18:00 universal time from June 2018 to July 2019. There are 37 pressure levels from near ground to 1 hPa in vertical direction. The surface data selected 10 metre U wind component, 10 metre V wind component, 2 metre dewpoint temperature, 2 metre temperature, mean sea level pressure, sea surface temperature, skin temperature, soil temperature and surface pressure. The pressure level data selected geopotential, relative humidity, specific humidity, temperature, U components of wind and V component of wind. These pressure level data and surface data are saved as the format of GRIB, which can be used as the initial field file of numerical model to simulate and forecast.

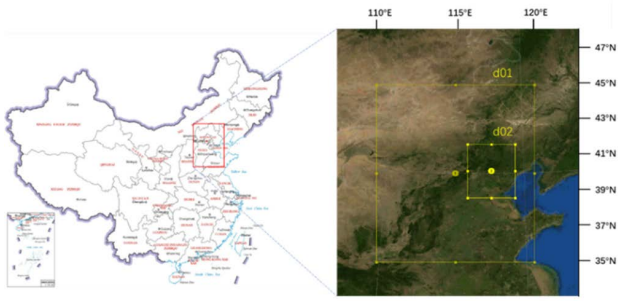

FIGURE 2. Diagram of double grid nesting in WRF.

The numerical model WRF is used to simulate and forecast the wind field in Beijing-Tianjin-Hebei-region. Considering the impact of actual geography on wind field forecast in Beijing-Tianjin-Hebei region, the double grid nesting is adopted in the study. The pressure level data and surface data provided by ERA-interim are used as the initial fields of the simulation, and the double grid nesting are marked as d01 and d02 respectively.

The calculation domain of the first grid d01 covers the whole Beijing-Tianjin-Hebei region, so as to simulate the wind field of the whole Beijing-Tianjin-Hebei region. The prediction results of wind field of this region are provided.

The grid d02 selects the low and gentle terrain in Beijing-Tianjin-Hebei region, mainly including Beijing, Tianjin and parts of Hebei Province. Figure 2 shows the distribution of double grid nesting. This double grid nesting can reduce the error of pre-diction results of wind field due to terrain difference. The grid points distance is 10km. The time step is set to 30 seconds and the output time is set to 3 hours. It means that the result is output every 3 hours, and the end time is set to 12 hours. According to ETA coordinates, the grid is divided into 38 layers in vertical height.

We applied the following physical parameterization schemes: (1) the Dudhia (Dudhia, 1989) and the RRTM (Mlawer *et al.*, 1997) schemes for shortwave and long-wave radiation, respectively; (2) the Lin scheme (Lin *et al.*, 1983) for microphysics; (3) the Kain-Fritsch scheme (Kain and Fritsch, 2002) for cumulus physics; (4) the Mellor-Yamada Janjić Scheme for the planetary boundary layer; and (5) the Noah LSM scheme (Tewari *et al.*, 2004) for the land surface processes.

Figure 3 and Figure 4 show statistic of wind speed and direction in the middle of the simulation domain, located at 115°E, 40°N at 650m above the local area from June 2018 to July 2019. The latitudinal wind is east-west and the westerly wind is positive; The longitudinal wind is north-south, and the south wind is positive. The figures show that at this location, the proportion of latitudinal wind below 2 m/s is the highest, the wind speed is not more than 6 m/s most of the time, and the proportion of westerly wind is highest in 13 months; The proportion of longitudinal wind from 2 m/s to 6 m/s is the

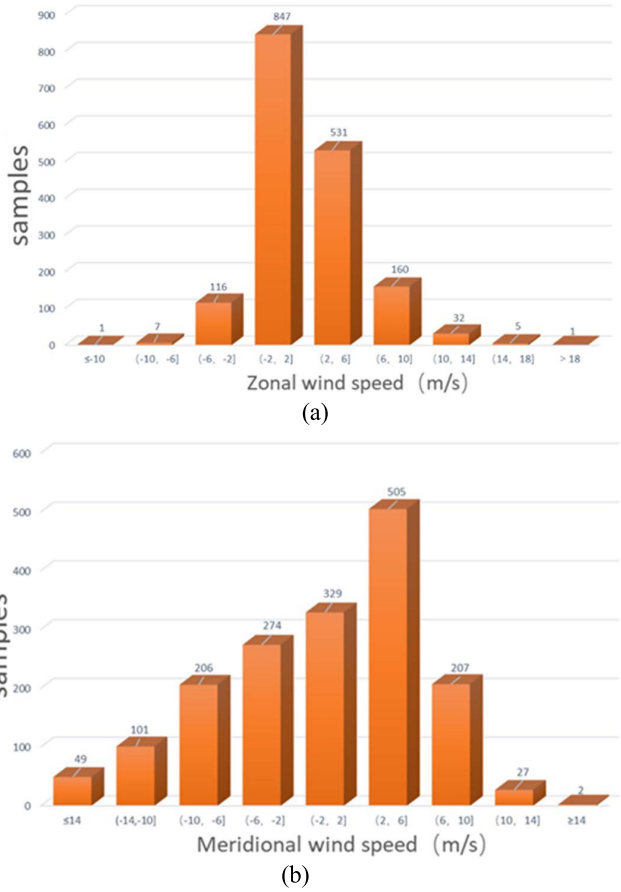

FIGURE 3. Distribution statistics of (a) zonal wind speed and (b) meridional wind speed.

highest. On the whole, the proportion of south wind and north wind in the whole year is roughly the same. Moreover, the time of south wind speed less than 6 m/s is longer than that of north wind speed less than 6 m/s. Figure 4 shows that the annual wind direction of this location is mostly southwest wind and northwest wind, and sometimes a small amount of southeast wind.

The simulation and statistical results are only 13 months' statistical data of a certain position over the Beijing-Tianjin-Hebei region and cannot represent the distribution of overall wind field. However, as the result of forecasting the wind field at a certain position, the result of numerical model can fulfill the task and requirements of forecasting wind field and provide dataset for the machine learning.

B. TRAINING PROCESS

There are many meteorological parameters in the initial field and forecast field files of the numerical model, but not all of them have great effects on the forecast of wind field. On the contrary, too many factors with low correlation will impact the training effect and speed of neural network. In many studies, temperature, humidity and pressure are the most important factors forecasting the wind field. In the training process, the temperature, humidity and pressure from

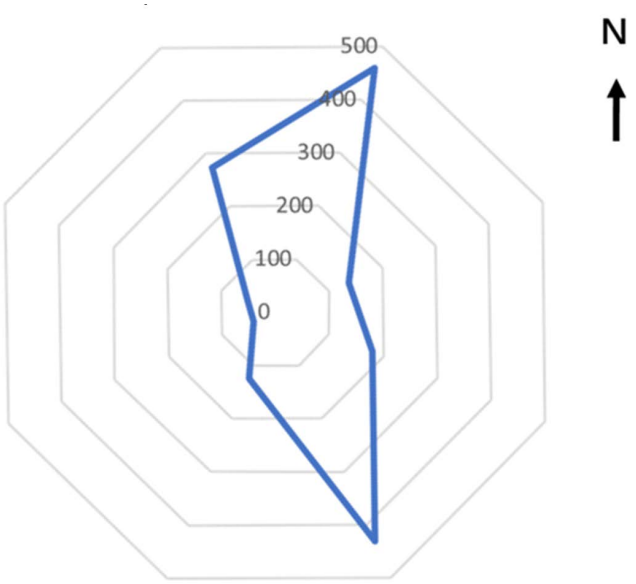

FIGURE 4. Distribution statistics of the wind direction.

ERA-interim data are used as the input of the neural network, and the wind speed and direction predicted by numerical model in 3 hours, 6 hours and 12 hours are used as the output of the neural network. Meridional wind, zonal wind and wind direction are trained and predicted separately by different machine learning models. The number of samples in the data set used in this paper is only 1700. However, it is very difficult to make tens of thousands or even millions of samples through WRF numerical simulation. In addition, many research has also achieved good results with few samples [54]–[57] Therefore, we think that 1700 samples are not too many, they can also reflect a certain law of wind field change.

In order to avoid the poor generalization ability of neural network model caused by data features and reduce the error, the data needs to be preprocessed. The range of input values is not consistent, and the data deviation is too large, which are not conducive to neural network processing. Therefore, this study uses normalization to solve the problem of poor training performance and training speed caused by different range of sample data, and it can eliminate the influence of dimension. After normalizing the data of temperature, humidity and pressure, the range of these variables is reduced to [0,1]. The formula of the normalized new variable A' is shown in equation (13):

$$A' = \frac{A - \min(A)}{\max(A) - \min(A)}, \tag{13}$$

where $\min\min(A)$ signifies the minimum value of variable A, and $\max(A)$ signifies the maximum value of variable A.

The temperature, humidity and pressure of the grid point around the forecast position extracted from the initial field file are used as the input of the neural network, and the wind speed and direction predicted by numerical model in 3 hours, 6 hours and 12 hours are used as the output of the neural network. The dataset is divided into training set and test set according to the ratio of 6:4, 7:3, 8:2 and 9:1. Meteorological data contains autocorrelations and the split is not random. Therefore, we divide the data set into ten parts in chronological order. Select the data of several consecutive adjacent time periods as the training set, and the rest as the test set. Since the training set can select more than one starting time period, the best training performance is selected as the training effect of this ratio. Three kinds of neural networks are selected: Long Short-Term Memory (LSTM), Convolutional Neural Networks (CNN) and DNN to be trained with the dataset. In this paper, the activation function of three kinds of neural networks is ReLU function. This is because the ReLU function can control the activation of neurons, and the gradient descent and back propagation efficiency of ReLU function is higher than other activation functions in gradient descent and back propagation, which can effectively avoid gradient explosion and gradient disappearance. According to the results of each training process, the weights and thresholds of the neural network are updated, so as to reduce the prediction error. The prediction error will remain stable. After that, the test set is input into the neural network, and the predicted value is compared with the actual value to evaluate whether the model is also effective for the test set data. Finally, the prediction results of different neural networks are compared, and the best neural network model is selected.

C. PREDICTION PROCESS IN APPLICATION

After trained and tested, the optimal machine learning model can be applied to the practical prediction. The source of the input data of the model in actual prediction process is different from that in the training process. As GNSS-RO data has the advantages of high precision and all-weather in providing global uniform distribution and high vertical resolution temperature, humidity and pressure profiles, it is selected for prediction when the model is applied to the practical prediction. It should be noted that ERA-interim data is used as the background field in the inversion of temperature, humidity and pressure data from GNSS-RO. This method of developing a skillful model and taking the rich data calculated by the model as the training starting point for machine learning model is called transfer learning. On some problems where you may not have so much data, it is used to develop the machine learning models with enough data [58], [19]

In practical application, temperature, humidity and pressure are extracted from GNSS-RO data as inputs of neural network, and the wind speed and direction can be predicted by the optimal neural network model. The data set from GNSS is used to confirm that the model can be used to predict the wind field from GNSS data. It is an-other testing dataset, different from the dataset from WRF. Figure 5 shows the process of the prediction of wind field.

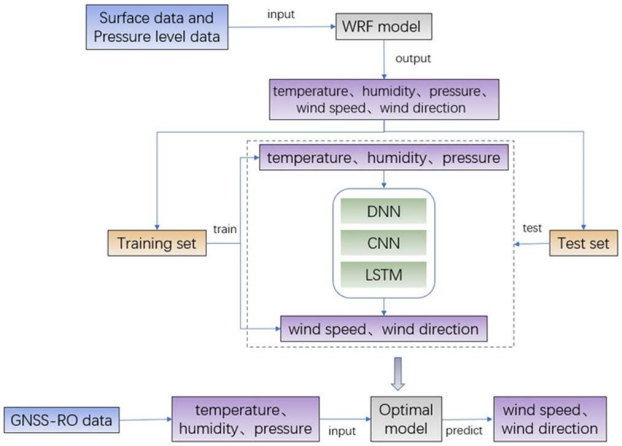

FIGURE 5. Process of prediction.

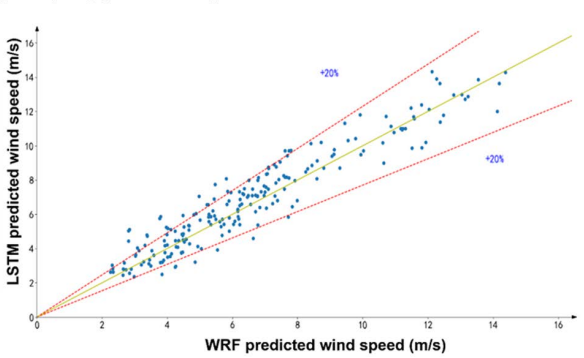

FIGURE 6. Comparison between WRF predicted wind speed and the LSTM predicted wind speed.

IV. RESULTS AND DISCUSSION

A. MODEL VERIFICATION AND COMPARISON

Take the position as an example, which is the center of the simulation domain located at 115°E, 40°N, 650 meters above the ground. When the height is less than 650m, the prediction accuracy will be affected by the interference of ground factors. When the height is more than 650m, the height difference between two adjacent isobaric surfaces is greater than 200m, which also affects the prediction accuracy. Therefore, the height of the position should not be too high. 650 meters is an appropriate height in this study. Figure 6 shows the LSTM wind speed based on the initial field of the WRF (Y-axis) against the WRF predicted wind speed (X-axis). The dots are not the full testing dataset. We selected the data from February and July 2019 to show, consistent with Figures 7, 8, 9 and 10. During the model training, the samples of wind field prediction come from the simulation result of numerical model. Therefore, the figure also shows the comparison between the neural network and the numerical model. The ordinate signifies the predicted value of LSTM and the abscissa signifies the wind speed value from WRF prediction. Under the ideal condition, the predicted wind speed of the neural network and the value from test set should be equal, and the scatter point should be near the yellow line of y=x. The closer the point in the figure is to the line y=x, the closer the predicted value is to the simulated value. Therefore, the prediction performance of neural network can be evaluated from the distribution of the point in the figure. It can be seen from the figure that most of the points are near y=x, and the error is within 20%. It indicates that the neural network has a gratifying prediction performance.

Figure 7, figure 8 and Figure 9 show the wind field prediction results of wind field with LSTM, CNN and DNN. In these figures, u is the actual zonal wind speed of samples; u-3h is the predicted zonal wind speed at that current moment by the machine learning model that is predicted using the meteorological parameters three hours ago. Similarly, v is the meridional wind speed of samples; v-3h is the predicted meridional wind speed that is predicted using the meteorological parameters three hours ago.

The figures show that for the three kinds of neural networks, the predicted wind field in 3 hours and 6 hours has little deviation from the wind field of test set. Three kinds of neural networks have huge deviations when predicting wind field in 12 hours. In other words, the three kinds of neural networks have no ability to predict the wind field after 12 hours. The prediction ability of neural network gradually decreases with time going on, and it completely loses its prediction ability in 12 hours. In addition, the figures show that the prediction performances of CNN and LSTM are similar, and they are obviously better than DNN. It also shows that LSTM has certain advantages in prediction of time series, and CNN has more advantages in three-dimensional data processing. The two kinds of neural networks have their own optimization effect on the prediction of wind field in this study.

Whether LSTM or CNN, the prediction error of wind field is smaller than that of DNN. LSTM and CNN have similar prediction effect due to their respective ad-vantages in data processing and algorithm. The two models have good prediction performance in wind field prediction in 3 hours: The prediction error of wind speed is about 1.4m/s, and the prediction error of wind direction is about 30 °. In addition, the prediction errors of prediction results in 3 hours are small, and the prediction errors of neural network will be larger and larger with time. The three neural networks have no prediction ability for wind field over 12 hours.

B. COMPARISON BETWEEN PREDICTION VALUES AND ACTUAL VALUES

According to the comparison of numerical simulation and machine learning pre-diction results, it is proved that the prediction results of machine learning model, especially LSTM and CNN, are similar to those of numerical model. In order to verify that the machine learning model can be applied in practice, it is necessary to compare the predicted results with the actual monitoring values of wind field. If the prediction results of the two prediction methods are close to

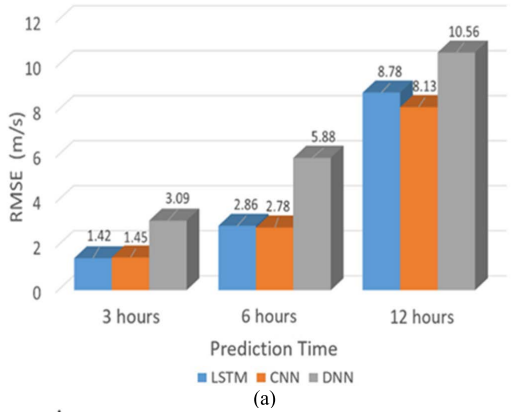

(a)

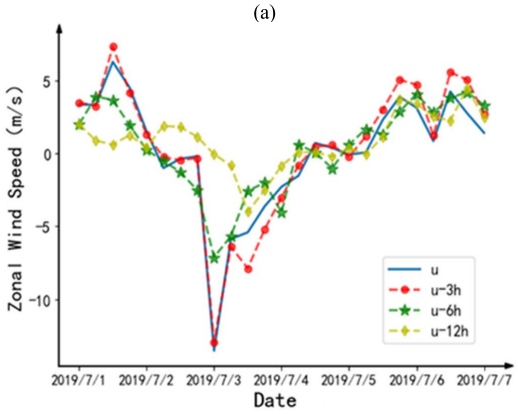

(b)

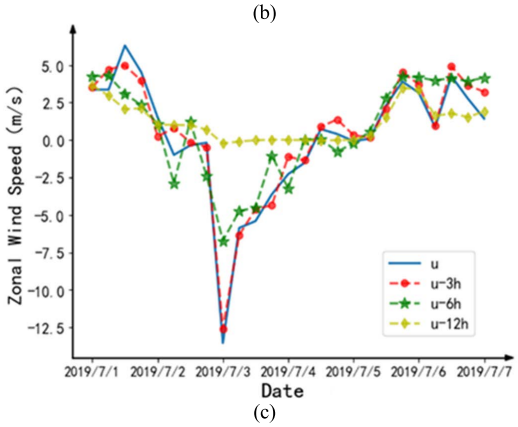

(c)

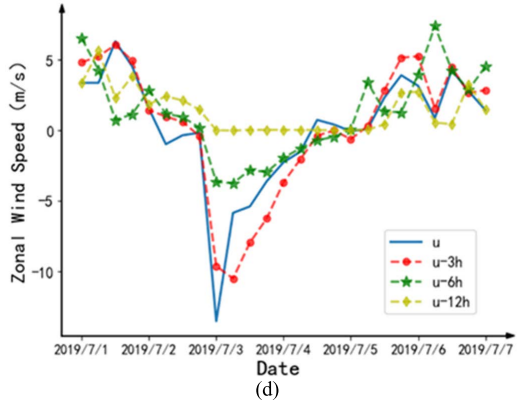

(d)

FIGURE 7. Prediction results of Zonal wind speed by different prediction models. (a) RMSE of zonal wind speed, (b) prediction results of zonal wind speed of LSTM, (c) prediction results of zonal wind speed of CNN, (d) prediction results of zonal wind speed of DNN.

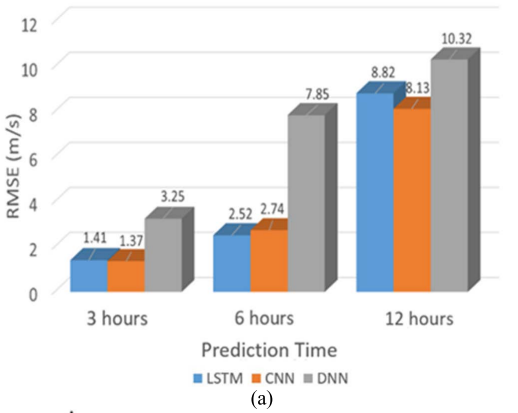

(a)

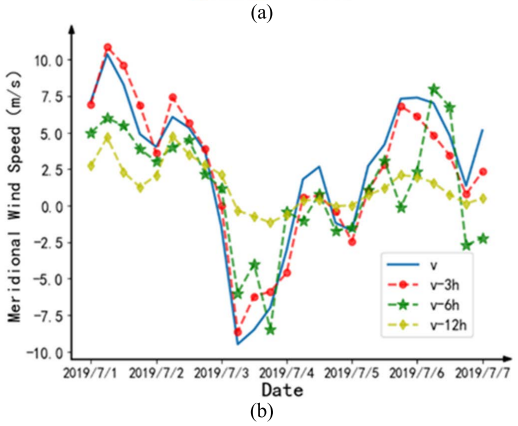

(b)

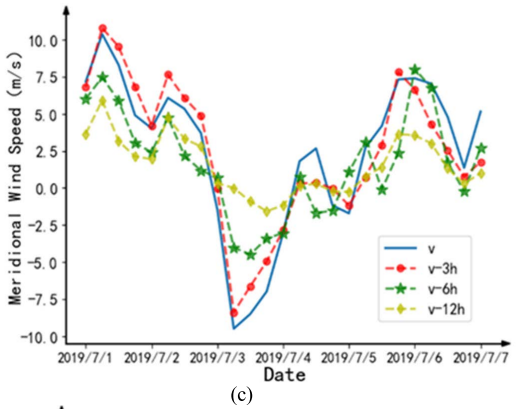

(c)

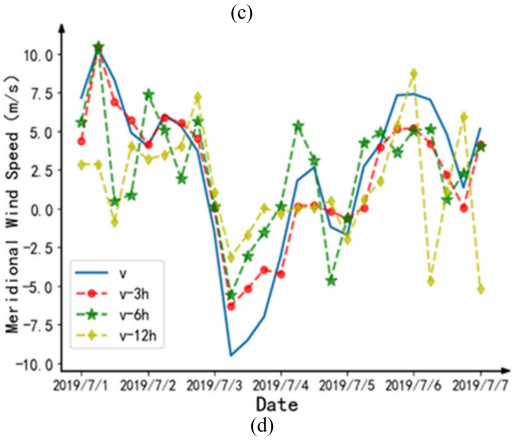

(d)

FIGURE 8. Prediction results of meridional wind speed by different prediction models. (a) RMSE of Meridional wind speed, (b) pre-diction results of Meridional wind speed of LSTM, (c) prediction results of Meridional wind speed of CNN, (d) prediction results of Meridional wind speed of DNN.

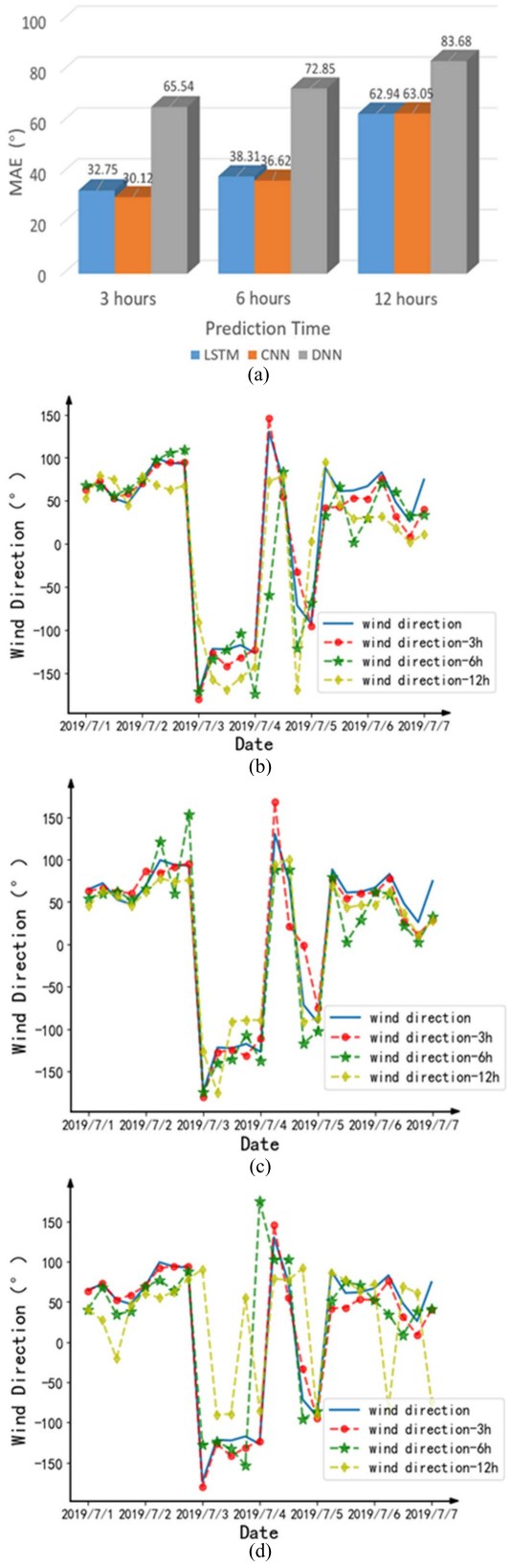

FIGURE 9. Prediction results of the wind direction by different prediction models. (a) MAE of wind direction, (b) prediction results of wind direction of LSTM, (c) prediction results of wind direction of CNN, (d) prediction results of wind direction of DNN.

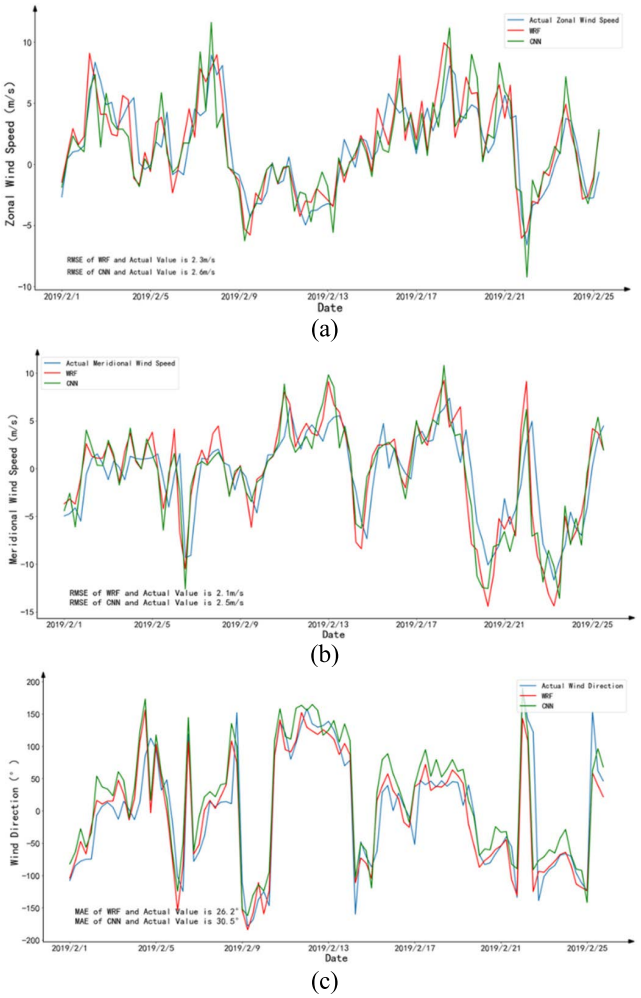

FIGURE 10. Comparison of predicted and monitored values of wind field. (a) Zonal wind speed of monitored values,WRF and CNN, (b) meridional wind speed of monitored values,WRF and CNN, (c) wind direction of monitored values,WRF and CNN.

the actual monitoring values of wind field, it verifies that the machine learning has a good prediction performance and can be applied to the actual wind field prediction.

Since the ERA-interim data of ECMWF has the shortest time interval of 6 hours, that is, there is only one monitoring data at least every 6 hours, this paper compared the prediction results of machine learning and numerical model with the actual monitoring values in 6 hours. The comparison is shown in Figure 10. Different from the previous conclusion, we show the figure from February here because it is better displayed here and can highlight the relationship among the three variables.

Table 1 shows that compared with the actual monitoring value of wind field, the prediction errors of wind speed in 6 hours of prediction models, whether WRF or ma-chine learning, are less than 3m/s, and the prediction error of wind direction is about 30 °. The prediction results of numerical model and machine learning model are close to the actual

TABLE 1. Comparison of errors between predicted and monitored values.

Model	RMSE(m/s)		MAE(°)
	Zonal Wind Speed	Meridional Wind Speed	Wind Direction
WRF	2.3	2.1	26.2
CNN	2.6	2.5	30.5
LSTM	2.7	2.4	31.6

wind field, which shows that the two prediction models can accurately predict the actual wind field.

C. THE EFFECT OF PARTITION OF DATASET ON PREDICTION RESULTS

The ultimate goal of machine learning is to apply the trained machine learning model to actual practice. The model must have excellent prediction ability in actual practice and smaller error compared with the real value. If the number of samples is large enough, the division of training set and test set will not have a great impact on the prediction performance. But when the number of samples is not large enough, it is necessary to adjust the ratio of training set to test set to improve the prediction performance. In this study, the ratio of training set to test set is adjusted under the condition of other parameters fixed. Figure 11 shows the influence of different division proportion on prediction performance. It can be seen from the figure that when the ratio of training set to test set is 8:2, RMSE and MAE of the model is the smallest, which is the best partition ratio. When the proportion of training set is too low, the prediction performance is not good because there is no enough samples for training; When the ratio is more than 8:2, the proportion of test set is too low, which cannot reflect the real training effect. Therefore, 8:2 is the best ratio of training set to test set in this study.

D. COMPARISON OF TRAINING TIME AND PREDICTION TIME

The training time reflects the training speed of different machine learning models. The prediction time reflects the computing time of different models. The shorter the prediction time is, the shorter the time from data input to prediction results output is, and it can better meet some specific requirements of timeliness information. The numerical model also needs to be tested to compare the difference of prediction time be-tween machine learning model and traditional weather simulation model. Table 2 shows the training time and prediction time of different models.

Due to the different structure of the models, among the three machine learning models, DNN has the shortest training time and prediction time, and CNN has the longest training time and prediction time. Compared with the machine learning model, the numerical model does not need to be trained in advance, so it has no training time; However, the machine learning method only takes about 2 seconds to predict the wind field, and WRF takes 15 minutes. The

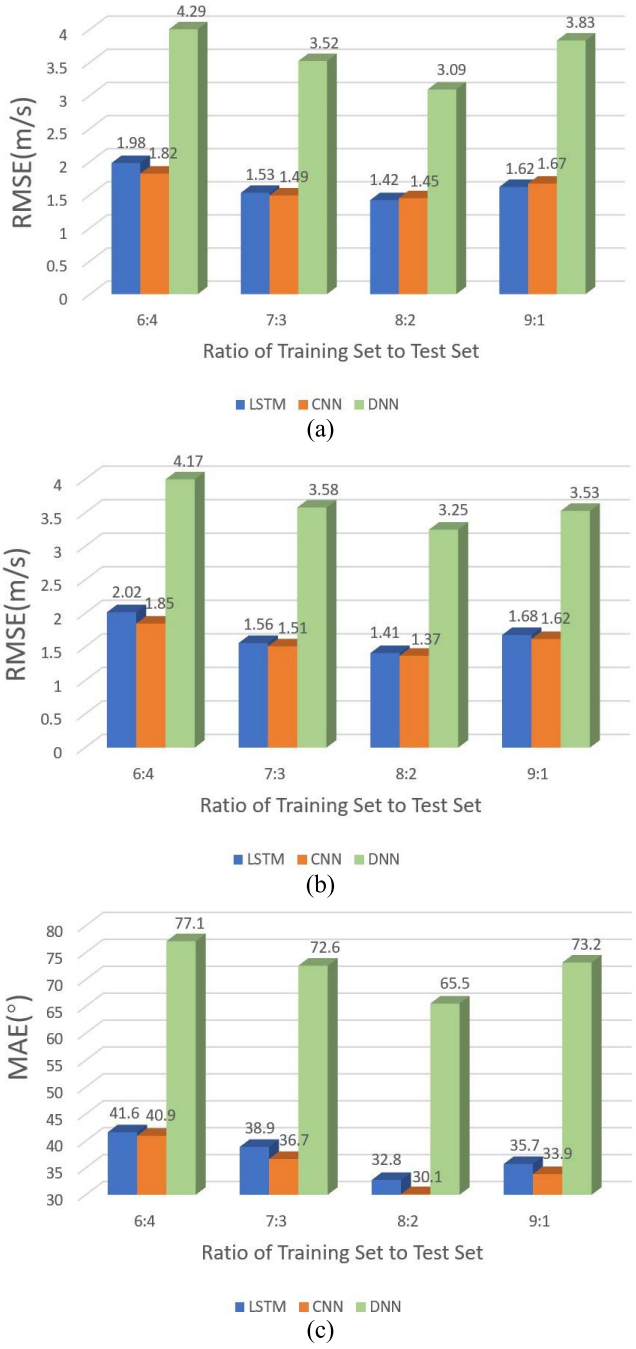

FIGURE 11. The influence of the ratio of dataset on the prediction performance. (a) RMSE of Zonal wind speed with different ratio of dataset, (b) RMSE of Meridional wind speed with different ratio of dataset, (c) MAE of wind direction with different ratio of dataset.

prediction time of machine learning is only 0.2% of WRF. The time of machine learning is much shorter than that of numerical model. In addition, the conditions required for numerical models are more complex than that for machine learning, including surface data and pressure level data with various necessary parameters, as well as complex operations such as making input files, configuring relevant parameters. However, machine learning only needs three atmospheric

TABLE 2. Training time and prediction time of different models.

	LSTM	CNN	DNN	WRF
Training Time	21min 3s	35min 26s	14min 41s	
Prediction Time	1.8s	2.2s	1.6s	15min 32s
Relative Prediction Time	0.19%	0.24%	0.17%	100%

parameters: temperature, humidity and pressure. All in all, the machine learning method can process the information in time and has great advantages in the timeliness of information.

E. VALIDATION OF MACHINE LEARNING FOR GNSS-RO DATA

In the process of model training and testing, the input data of temperature, humidity and pressure of the model come from ERA-interim dataset. In order to verify that the model has the same prediction performance on GNSS-RO data, it is necessary to validate the effectiveness of the model on GNSS-RO data.

One occultation event can only provide one occultation data profile of the position of the satellite at that time. Therefore, it is necessary to obtain the meteorological data in the prediction area from GNSS-RO by interpolation. Each occultation event is classified according to the periods. The period of at least seven occultation events occurred in Beijing Tianjin Hebei region during two hours is selected for interpolation of meteorological parameters. The temperature, humidity and pressure are interpolated according to the same grid distribution as ERA-interim, and the corresponding meteorological parameters (temperature, humidity and pressure) in longitude and latitude can be calculated. Figures 12, 13 and 14 show the distribution of temperature, humidity and pressure near the predicted position (115 ° E, 40 ° N), which are obtained by the interpolation of GNSS-RO data and the actual monitoring value separately.

The figures show that the meteorological parameters of the area obtained by interpolation of GNSS-RO data are close to the actual monitoring values, and the errors are less than 10%, which verifies the reliability of the interpolation to calculate meteorological parameters.

In application, the meteorological parameters obtained from interpolation of GNSS-RO data are used as the input of the machine learning model to predict the wind field. Figure 15 shows the prediction errors of the machine learning model with different numbers of occultation profiles. It shows that the more occultation profiles, the smaller the prediction error. When the number of occultation profiles is at least 7, the machine learning model have the similar prediction error and the error is close to that verified by the test set. This verifies that GNSS-RO data is effective for machine learning prediction.

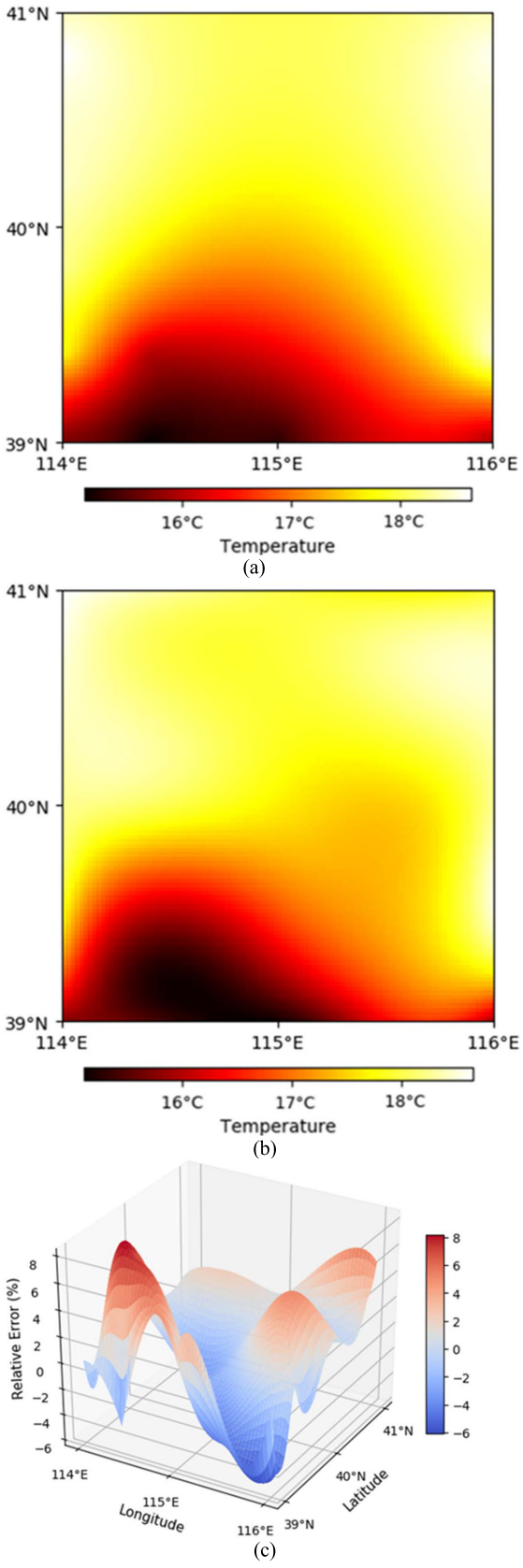

FIGURE 12. (a) Interpolation temperature of GNSS-RO data, (b)actual monitoring temperature and (c)the relative error between the temperature of interpolation and actual monitoring.

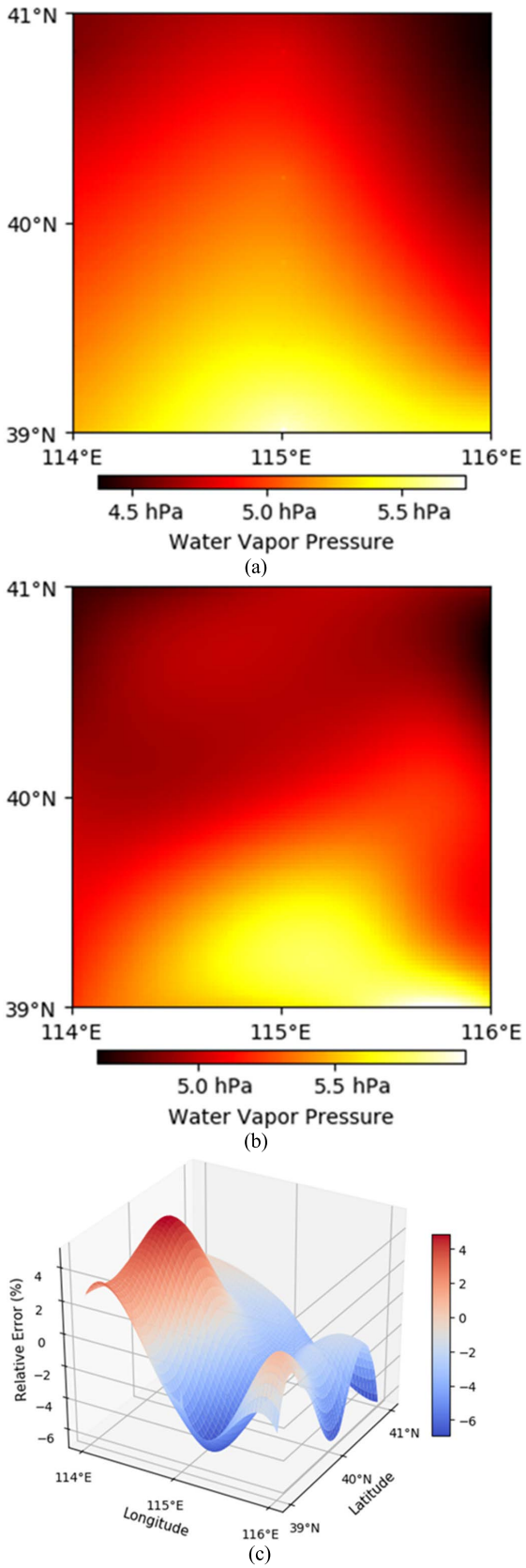

FIGURE 13. (a) Interpolation humidity of GNSS-RO data, (b)actual monitoring humidity and (c)the relative error between the humidity of interpolation and actual monitoring.

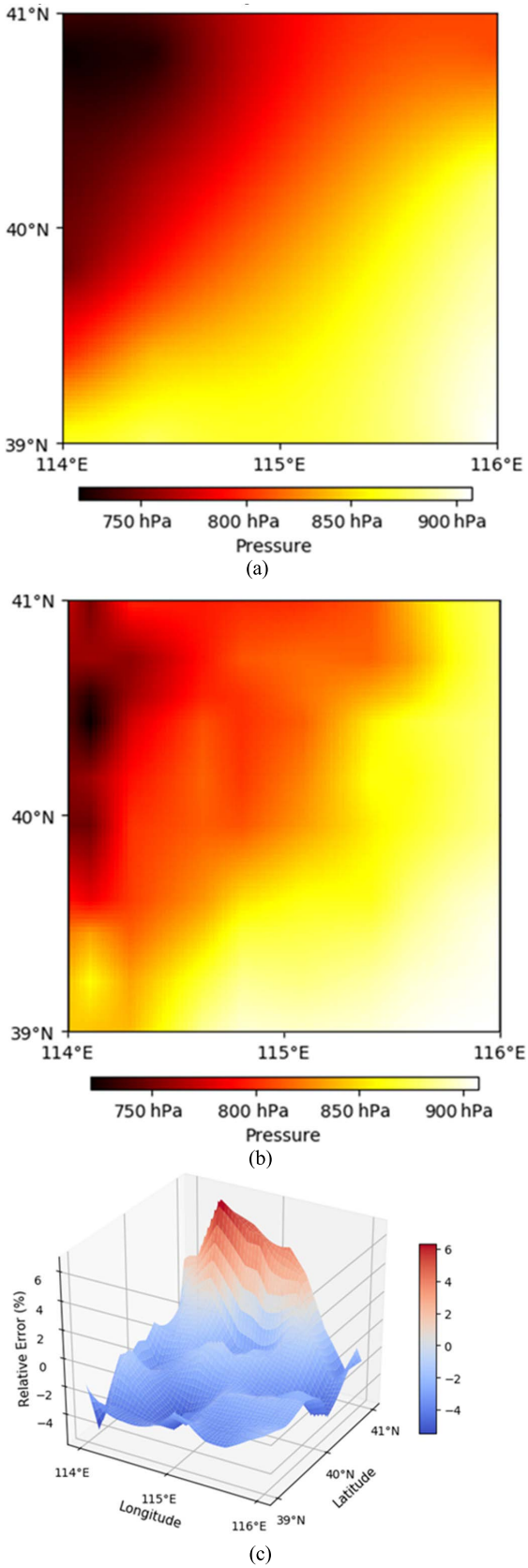

FIGURE 14. (a) Interpolation pressure of GNSS-RO data, (b)actual monitoring pressure and (c)the relative error between the pressure of interpolation and actual monitoring.

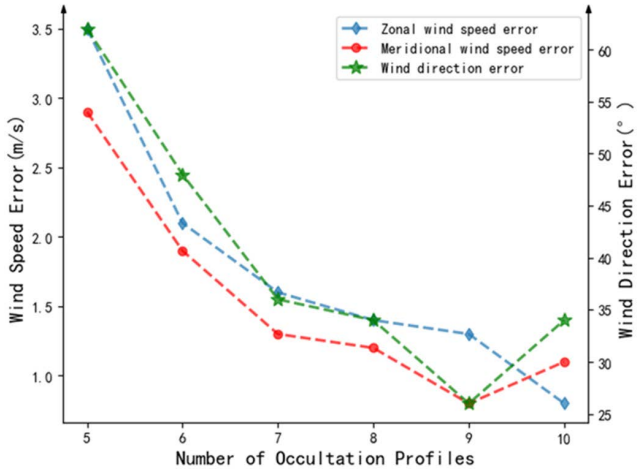

FIGURE 15. The prediction errors of the machine learning model with different numbers of occultation profiles.

V. CONCLUSION

This paper provides a machine learning-based method to predict regional wind field utilizing GNSS-RO data. For remote sensing observation, sometimes we can only obtain thermodynamic parameters due to the limitation of instruments carried by satellites. We used machine learning method to establish the relationship between thermodynamic parameters and kinetic parameters and we can predict kinetic parameters only by using thermodynamic parameters, which is impossible only using numerical model. Firstly, the numerical model WRF is used to simulate and predict the wind field over Beijing-Tianjin-Hebei region, and it provides the datasets including temperature, humidity, pressure, wind speed and direction. Secondly, different machine learning models are established to capture the relationship between meteorological parameters and wind field. The transfer learning solves the problem that the machine learning model cannot achieve good training performance due to the insufficient sample of GNSS-RO. Finally, the GNSS-RO data is used to predict the wind field through the trained machine learning model. The number of samples in the data set used in this paper is only 1700. In the follow-up study, if we can expand the number of samples, it will be a good choice. Especially with the development of micro-nano satellite technology, GNSS radio occultation will soon achieve constellation detection of a scale of hundreds of satellites. At that time, the huge amount of occultation data is expected to bring great changes to numerical prediction. By the analysis of the results, the following conclusions can be drawn:

1. Machine learning has a good performance in predicting wind field. The error be-tween machine learning and numerical model is very small. Among the neural networks, LSTM and CNN have smaller prediction error than DNN. When predicting the wind field in 3 hours, the wind speed error of LSTM and CNN is about 1.4 m/s and the wind direction error is 30°. Compared with DNN, the wind speed error of LSTM and CNN is reduced by 57% and the wind direction error is reduced by 50%. The longer the prediction time, the greater the prediction error.

2. The error between the prediction results of machine learning model and the actual monitoring values of wind field is very small. In the 6-hour wind field prediction, the wind speed error between the prediction results in 6 hours of machine learning and the actual monitoring value is about 2.5m/s, and the wind direction error is about 30°. It shows that the machine learning model has good performance on predicting the actual wind field, which verifies the reliability of the machine learning method.

3. The dataset has a certain influence on the prediction performance. Through the comparison of training effect under different division methods of datasets, more effective machine learning models are screened out. After testing and comparing, it is found that when the ratio of training set to test set is 8:2, the prediction performance is the best.

4. Machine learning and the numerical model have similar prediction performance, but the prediction time required by machine learning is only 0.2% compared with the numerical model. The prediction speed is far higher than that of the numerical model. It shows that machine learning method has great advantages in the timeliness of information. In addition, the prediction conditions required for numerical models are more complex than machine learning. The machine learning meth-od only needs three atmospheric parameters: temperature, humidity and pressure.

5. The interpolated GNSS-RO data is used as the input data of machine learning model in application, and the prediction performance is excellent. The requirement of meteorological data acquisition including temperature, pressure and humidity from GNSS-RO data is occultation occurs at least seven times during two hours. The error between the interpolation result and the actual monitoring value is less than 10%. The interpolated meteorological parameters are used for machine learning prediction of wind field. The prediction error is close to that of the test set. It is verified that GNSS-RO data can be used in practical application to predict the wind fields by machine learning model.

REFERENCES

[1] V. O. K. Li, J. C. K. Lam, Y. Han, and K. Chow, "A big data and artificial intelligence framework for smart and personalized air pollution monitoring and health management in Hong Kong," *Environ. Sci. Policy*, vol. 124, pp. 441–450, Oct. 2021, doi: 10.1016/j.envsci.2021.06.011.

[2] W. U. Meng, L. U. O. Yun, Z. Yan-Ping, W. Xiao-Xun, F. Shao-Jia, and W. Dui, "Study of the vertical wind field structure and its relationship with $PM_{(2.5)}$ air pollution over the pearl river delta in autumn," *J. Trop. Meteorol.*, vol. 26, pp. 82–92, Mar. 2020.

[3] B. Wang, C. M. Zhang, F. D. Liu, Y. Yang, L. Wang, R. P. Guo, Y. H. Qiao, Y. Y. Liu, S. Q. Yu, and Q. Zhang, "Review on the application of numerical weather prediction in the simulation research of atmospheric dispersion," *Adv. Mater. Res.*, vols. 953–954, pp. 428–431, Jun. 2014, doi: 10.4028/www.scientific.net/amr.953-954.428.

[4] W. G. Melbourne, E. S. Davis, T. P. Yunck, and B. D. Tapley, "The GPS flight experiment on TOPEX/POSEIDON," *Geophys. Res. Lett.*, vol. 21, no. 19, pp. 2171–2174, Sep. 1994, doi: 10.1029/94GL02192.

[5] E. R. Kursinski, G. A. Hajj, J. T. Schofield, R. P. Linfield, and K. R. Hardy, "Observing Earth's atmosphere with radio occultation measurements using the global positioning system," *J. Geophys. Res., Atmos.*, vol. 102, no. D19, pp. 23429–23465, Oct. 1997, doi: 10.1029/97JD01569.

[6] M. J. Mueller, A. C. Kren, L. Cucurull, S. P. F. Casey, R. N. Hoffman, R. Atlas, and T. R. Peevey, "Impact of refractivity profiles from a proposed GNSS-RO constellation on tropical cyclone forecasts in a global modeling system," *Monthly Weather Rev.*, vol. 148, no. 7, pp. 3037–3057, Jul. 2020, doi: 10.1175/mwr-d-19-0360.1.

[7] S. Allabakash and S. Lim, "Climatology of planetary boundary layer height-controlling meteorological parameters over the Korean peninsula," *Remote Sens.*, vol. 12, no. 16, p. 2571, Aug. 2020, doi: 10.3390/rs12162571.

[8] Y. A. Liou, A. G. Pavelyev, C. Y. Huang, K. Igarashi, K. Hocke, and S. K. Yan, "Analytic method for observation of the gravity waves using radio occultation data," *Geophys. Res. Lett.*, vol. 30, no. 20, pp. 1–5, Oct. 2003, doi: 10.1029/2003GL017818.

[9] Y. Ying and F. Zhang, "Potentials in improving predictability of multiscale tropical weather systems evaluated through ensemble assimilation of simulated satellite-based observations," *J. Atmos. Sci.*, vol. 75, no. 5, pp. 1675–1698, May 2018, doi: 10.1175/JAS-D-17-0245.1.

[10] J.-F. Li, K. Xu, J. H. Jiang, W. Lee, L. Wang, J. Yu, G. Stephens, E. Fetzer, and Y. Wang, "An overview of CMIP5 and CMIP6 simulated cloud ice, radiation fields, surface wind stress, sea surface temperatures, and precipitation over tropical and subtropical oceans," *J. Geophys. Res., Atmos.*, vol. 125, no. 15, Aug. 2020, Art. no. e2020JD032848, doi: 10.1029/2020JD032848.

[11] X. Xie, S. Zhou, J. Zhang, and P. Huang, "The role of background SST changes in the ENSO-driven rainfall variability revealed from the atmospheric model experiments in CMIP5/6," *Atmos. Res.*, vol. 261, Oct. 2021, Art. no. 105732.

[12] L. Quitián-Hernández, P. Bolgiani, D. Santos-Muñoz, M. Sastre, J. Díaz-Fernández, J. J. González-Alemán, J. I. Farrán, L. Lopez, F. Valero, and M. L. Martín, "Analysis of the October 2014 subtropical cyclone using the WRF and the HARMONIE-AROME numerical models: Assessment against observations," *Atmos. Res.*, vol. 260, Oct. 2021, Art. no. 105697, doi: 10.1016/j.atmosres.2021.105697.

[13] Y. Wang and S. M. Quiring, "Impact of soil moisture initializations on WRF-simulated north American monsoon system," *J. Geophys. Res., Atmos.*, vol. 126, no. 4, Feb. 2021, Art. no. e2020JD033858, doi: 10.1029/2020JD033858.

[14] R. Pokhrel, S. D. Cos, J. P. Montoya Rincon, E. Glenn, and J. E. González, "Observation and modeling of hurricane Maria for damage assessment," *Weather Climate Extremes*, vol. 33, Sep. 2021, Art. no. 100331, doi: 10.1016/j.wace.2021.100331.

[15] J. Díaz-Fernández, P. Bolgiani, D. Santos-Muñoz, M. Sastre, F. Valero, L. I. Sebastián-Martín, S. Fernández-González, L. López, and M. L. Martín, "On the characterization of mountain waves and the development of a warning method for aviation safety using WRF forecast," *Atmos. Res.*, vol. 258, Aug. 2021, Art. no. 105620, doi: 10.1016/j.atmosres.2021.105620.

[16] C. Yang, L. Zhu, and J. Min, "Impact study of FY-3B MWRI data assimilation in WRFDA," *Atmosphere*, vol. 12, no. 4, p. 497, Apr. 2021, doi: 10.3390/atmos12040497.

[17] Q. Zhang, C. Wei, Y. Wang, S. Du, Y. Zhou, and H. Song, "Potential for prediction of water saturation distribution in reservoirs utilizing machine learning methods," *Energies*, vol. 12, no. 19, p. 3597, Sep. 2019, doi: 10.3390/en12193597.

[18] H. Song, S. Du, R. Wang, J. Wang, Y. Wang, C. Wei, and Q. Liu, "Potential for vertical heterogeneity prediction in reservoir basing on machine learning methods," *Geofluids*, vol. 2020, pp. 1–12, Aug. 2020, doi: 10.1155/2020/3713525.

[19] S. Du, R. Wang, C. Wei, Y. Wang, Y. Zhou, J. Wang, and H. Song, "The connectivity evaluation among wells in reservoir utilizing machine learning methods," *IEEE Access*, vol. 8, pp. 47209–47219, 2020, doi: 10.1109/ACCESS.2020.2976910.

[20] J. Lv, X. Zheng, M. Pawlak, W. Mo, and M. Miśkowicz, "Very short-term probabilistic wind power prediction using sparse machine learning and nonparametric density estimation algorithms," *Renew. Energy*, vol. 177, pp. 181–192, Nov. 2021, doi: 10.1016/j.renene.2021.05.123.

[21] D. Gupta, N. Natarajan, and M. Berlin, "Short-term wind speed prediction using hybrid machine learning techniques," *Environ. Sci. Pollut. Res.*, Jul. 2021, doi: 10.1007/s11356-021-15221-6.

[22] A. H. Işik, F. K. D. Örgen, C. Şirin, A. D. Tuncer, and A. Güngör, "Prediction of wind blowing durations of Eastern Turkey with machine learning for integration of renewable energy and organic farmingstock raising," *Sci. J. Mehmet Akif Ersoy Univ.*, vol. 2, no. 3, pp. 47–53, Sep. 2019.

[23] A. Mercer and J. Dyer, "A new scheme for daily peak wind gust prediction using machine learning," *Proc. Comput. Sci.*, vol. 36, pp. 593–598, Jan. 2014, doi: 10.1016/j.procs.2014.09.059.

[24] J. Wang, Y. Song, F. Liu, and R. Hou, "Analysis and application of forecasting models in wind power integration: A review of multi-step-ahead wind speed forecasting models," *Renew. Sustain. Energy Rev.*, vol. 60, pp. 960–981, Jul. 2016, doi: 10.1016/j.rser.2016.01.114.

[25] M. Neshat, M. M. Nezhad, E. Abbasnejad, S. Mirjalili, L. B. Tjernberg, D. A. Garcia, B. Alexander, and M. Wagner, "A deep learning-based evolutionary model for short-term wind speed forecasting: A case study of the lillgrund offshore wind farm," *Energy Convers. Manage.*, vol. 236, May 2021, Art. no. 114002, doi: 10.1016/j.enconman.2021.114002.

[26] Y. Dong, J. Wang, L. Xiao, and T. Fu, "Short-term wind speed time series forecasting based on a hybrid method with multiple objective optimization for non-convex target," *Energy*, vol. 215, Jan. 2021, Art. no. 119180, doi: 10.1016/j.energy.2020.119180.

[27] K. Shivam, J.-C. Tzou, and S.-C. Wu, "Multi-step short-term wind speed prediction using a residual dilated causal convolutional network with nonlinear attention," *Energies*, vol. 13, no. 7, p. 1772, Apr. 2020, doi: 10.3390/en13071772.

[28] H. Ando, T. Imamura, S. Tellmann, M. Pätzold, B. Häusler, N. Sugimoto, M. Takagi, H. Sagawa, S. Limaye, Y. Matsuda, R. K. Choudhary, and M. Antonita, "Thermal structure of the Venusian atmosphere from the sub-cloud region to the mesosphere as observed by radio occultation," *Sci. Rep.*, vol. 10, no. 1, pp. 1–7, Dec. 2020, doi: 10.1038/s41598-020-59278-8.

[29] O. I. Yakovlev, S. S. Matyugov, and A. A. Pavelyev, "Results of studying the daytime polar ionosphere by the radio occultation method on satellite-to-satellite paths," *Radiophys. Quantum Electron.*, vol. 62, no. 3, pp. 174–182, Aug. 2019, doi: 10.1007/s11141-019-09965-y.

[30] X. Hou, Y. Han, X. Hu, and F. Weng, "Verification of fengyun-3D MWTS and MWHS calibration accuracy using GPS radio occultation data," *J. Meteorol. Res.*, vol. 33, no. 4, pp. 695–704, Aug. 2019, doi: 10.1007/s13351-019-8208-9.

[31] X.-X. Ma, Z. Lin, H.-L. Jin, H.-R. Chen, and L.-G. Jiao, "Analysis of the temporal-spatial distribution of ionosphere scale height based on COSMIC occultation data," *Astrophys. Space Sci.*, vol. 362, no. 11, pp. 1–7, Nov. 2017, doi: 10.1007/s10509-017-3182-0.

[32] T. O. Myslivtsev, S. V. Nikiforov, A. I. Pogoreltsev, P. V. Savochkin, I. V. Sakhno, A. A. Semenov, and B. V. Troitsky, "Improving capabilities of broadband differential satellite navigation systems via radio occultation technology," *Geomagnetism Aeronomy*, vol. 56, no. 4, pp. 457–463, Jul. 2016, doi: 10.1134/S0016793216040137.

[33] Y. Liu and J. Xue, "Assimilation of global navigation satellite radio occultation observations in GRAPES: Operational implementation," *J. Meteorol. Res.*, vol. 28, no. 6, pp. 1061–1074, Dec. 2014, doi: 10.1007/s13351-014-4028-0.

[34] V. I. Zakharov and V. E. Kunitsyn, "Possibilities of radio occultation sounding using the GPS/GLONASS system for regional monitoring of the atmosphere," *Moscow Univ. Phys. Bull.*, vol. 62, no. 4, pp. 260–265, Aug. 2007, doi: 10.3103/S0027134907040133.

[35] J. Wickert, C. Reigber, G. Beyerle, R. König, C. Marquardt, T. Schmidt, L. Grunwaldt, R. Galas, T. K. Meehan, W. G. Melbourne, and K. Hocke, "Atmosphere sounding by GPS radio occultation: First results from CHAMP," *Geophys. Res. Lett.*, vol. 28, no. 17, pp. 3263–3266, Sep. 2001, doi: 10.1029/2001GL013117.

[36] A. K. Steiner, G. Kirchengast, and H. P. Ladreiter, "Inversion, error analysis, and validation of GPS/MET occultation data," *Annales Geophysicae*, vol. 17, no. 1, pp. 122–138, Jan. 1999, doi: 10.1007/s00585-999-0122-5.

[37] C. J. Johny, S. K. Sarkar, and D. Punyasesudu, "Atmospheric phenomena deduced from radiosonde and GPS occultation measurements for various application related studies," *J. Earth Syst. Sci.*, vol. 118, no. 1, pp. 49–59, Feb. 2009, doi: 10.1007/s12040-009-0005-x.

[38] M. V. Ratnam and S. G. Basha, "A robust method to determine global distribution of atmospheric boundary layer top from COSMIC GPS RO measurements," *Atmos. Sci. Lett.*, vol. 11, no. 3, pp. 216–222, Aug. 2010, doi: 10.1002/asl.277.

[39] G. Basha, P. Kishore, M. V. Ratnam, S. Ravindra Babu, I. Velicogna, J. H. Jiang, and C. O. Ao, "Global climatology of planetary boundary layer top obtained from multi-satellite GPS RO observations," *Climate Dyn.*, vol. 52, nos. 3–4, pp. 2385–2398, Feb. 2019, doi: 10.1007/s00382-018-4269-1.

[40] D. Jagadheesha, B. Manikiam, N. Sharma, and P. K. Pal, "Atmospheric stability index using radio occultation refractivity profiles," *J. Earth Syst. Sci.*, vol. 120, no. 2, pp. 311–319, Apr. 2011, doi: 10.1007/s12040-011-0053-x.

[41] E. L. Fleming, S. Chandra, J. J. Barnett, and M. Corney, "Zonal mean temperature, pressure, zonal wind and geopotential height as functions of latitude," *Adv. Space Res.*, vol. 10, pp. 11–59, Jan. 1990, doi: 10.1016/0273-1177(90)90386-E.
[42] M.-A. Sato, "A real time learning algorithm for recurrent analog neural networks," *Biol. Cybern.*, vol. 62, no. 3, pp. 237–241, Jan. 1990, doi: 10.1007/BF00198098.
[43] B. W. Hong, "On the set up to the number of hidden node of adaptive back propagation neural network," *J. Inf. Technol.*, vol. 5, no. 2, pp. 55–67, 2002.
[44] L. M. Reyneri and E. Filippi, "Modified backpropagation algorithm for fast learning in neural networks," *Electron. Lett.*, vol. 26, no. 19, p. 1564, 1990, doi: 10.1049/el:19901004.
[45] J.-S. Shawe-Taylor and D.-A. Cohen, "Linear programming algorithm for neural networks," *Neural Netw.*, vol. 3, p. 5, 1990, doi: 10.1016/0893-6080(90)90007-8.
[46] H. N. Jong, M. C. Seon, H. L. Sang, S. Y. Hyun, and R. M. Seung, "A mapping strategy of multilayered neural networks on multiprocessor and its distributed backpropagation algorithm," *J. Korea Inf. Sci. Soc.*, vol. 17, no. 3, pp. 343–353, 1990.
[47] J. L. Chen and J. E. Summers, "Deep convolutional neural networks for semi-supervised learning from synthetic aperture sonar (SAS) images," *J. Acoust. Soc. Amer.*, vol. 141, no. 5, p. 3963, May 2017, doi: 10.1121/1.4989020.
[48] P. Le Callet, C. Viard-Gaudin, and D. Barba, "A convolutional neural network approach for objective video quality assessment," *IEEE Trans. Neural Netw.*, vol. 17, no. 5, pp. 1316–1327, Sep. 2006, doi: 10.1109/TNN.2006.879766.
[49] K. Wang, X. Wang, L. Lin, M. Wang, and W. Zuo, "3D human activity recognition with reconfigurable convolutional neural networks," in *Proc. 22nd ACM Int. Conf. Multimedia*, Nov. 2014, pp. 97–106, doi: 10.1145/2647868.2654912.
[50] A. Kara, "Multi-step influenza outbreak forecasting using deep LSTM network and genetic algorithm," *Expert Syst. Appl.*, vol. 180, Oct. 2021, Art. no. 115153, doi: 10.1016/j.eswa.2021.115153.
[51] Y. Imrana, Y. Xiang, L. Ali, and Z. Abdul-Rauf, "A bidirectional LSTM deep learning approach for intrusion detection," *Expert Syst. Appl.*, vol. 185, Dec. 2021, Art. no. 115524, doi: 10.1016/j.eswa.2021.115524.
[52] J. D. Domingo, J. Gomez-Garcia-Bermejo, and E. Zalama, "Optimization and improvement of a robotics gaze control system using LSTM networks," *Multimedia Tools Appl.*, vol. 81, no. 3, pp. 3351–3368, 2021, doi: 10.1007/s11042-021-11112-7.
[53] F. A. Gers, J. Schmidhuber, and F. Cummins, "Learning to forget: Continual prediction with LSTM," *Neural Comput.*, vol. 12, no. 10, pp. 2451–2471, Oct. 2000, doi: 10.1162/089976600300015015.
[54] A. Hu and K. Zhang, "Using bidirectional long short-term memory method for the height of F2 peak forecasting from ionosonde measurements in the Australian region," *Remote Sens.*, vol. 10, no. 10, p. 1658, Oct. 2018, doi: 10.3390/rs10101658.
[55] S. Bonafoni, F. Pelliccia, and R. Anniballe, "Comparison of different neural network approaches for the tropospheric profiling over the inter-tropical lands using GPS radio occultation data," *Algorithms*, vol. 2, no. 1, pp. 31–45, Jan. 2009, doi: 10.3390/a2010031.
[56] S. A. Abdul-Wahab and S. M. Al-Alawi, "Assessment and prediction of tropospheric ozone concentration levels using artificial neural networks," *Environ. Model. Softw.*, vol. 17, pp. 219–228, Jan. 2002, doi: 10.1016/S1364-8152(01)00077-9.
[57] Z. Zeng, X. Hu, and X. Zhang, "Applying artificial neural network to the short-term prediction of electron density structure using GPS occultation data," *Geophys. Res. Lett.*, vol. 29, no. 9, p. 35, May 2002, doi: 10.1029/2001GL013656.
[58] H. Song, S. Du, R. Wang, J. Wang, Y. Wang, C. Wei, and Q. Liu, "Potential for vertical heterogeneity prediction in reservoir basing on machine learning methods," *Geofluids*, vol. 2020, pp. 1–12, Aug. 2020, doi: 10.1155/2020/3713525.

XUEZHAO CHU was born in Hebei, China, in 1996. He received the B.S. degree from Beihang University, in 2018. He is currently pursuing the M.S. degree in fluid mechanics with the Beijing University of Science and Technology. He is a member of the National and Local Joint Engineering Laboratory for Big Data Analysis and Computing Technology. His current research interests include big data analysis of GNSS radio occultation and machine learning.

WEIHUA BAI is currently a Professor with the National Space Science Center, Chinese Academy of Sciences. He also served as the Director or the Deputy Director in FY3 series GNOS and GNOSII missions. His current research interests include GNSS radio occultation and GNSS-R remote sensing techniques and their applications.

YUEQIANG SUN is currently a Professor with the National Space Science Center, Chinese Academy of Sciences. She devotes to develop GNSS remote sensing and space-borne spatial environment exploration technologies. She has been the principal investigator or the vice principal investigator of more than 20 missions/projects in manned space flight, FengYun, and national natural science foundation (863) areas. Her research interests include GNSS radio occultation, GNSS-R remote sensing techniques, atmospheric physics, ionospheric physics, magnetic physics, and space physics.

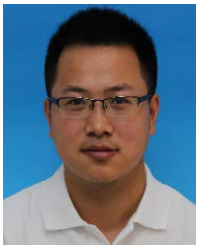

WEI LI is currently pursuing the Ph.D. degree with the National Space Science Center, Chinese Academy of Sciences. His research interests include GNSS radio occultation technique and GNSS remote sensing.

CONGLIANG LIU is currently a Doctor with the National Space Science Center, Chinese Academy of Sciences. His research interests include GNSS radio occultation technique and its meteorology and climate utilities and LEO-LEO microwave occultation technique.

HONGQING SONG was born in Liaoning, China, in 1982. He received the B.S. degree in chemical machinery from the Dalian University of Technology, in 2004, the degree in fluid mechanics (master and doctoral program) from the University of Science and Technology Beijing, in 2009, and the Ph.D. degree.

From 2014 to 2018, he was an Associate Professor with the School of Civil Engineering and Resource Engineering, University of Science and Technology Beijing. Since June 2018, he has been a Professor with the University of Science and Technology Beijing. He is currently a Professor with the University of Science and Technology Beijing and the Deputy Director of National and Local Joint Engineering Laboratory for Big Data Analysis and Computing Technology. He has authored two books, more than 100 scientific articles, and more than 15 inventions. His research interests include big data analysis and application in area of energy and environment, geo-energy reservoir modeling and simulation including oil/gas/thermal water, rainfall infiltration and runoff control for sponge city construction, groundwater flow and contaminant transport, and in-situ resource utilization in space.